

Geometric effects control isothermal oxidation of graphite flakes

Heinrich Badenhorst · Walter W. Focke

Received: 22 January 2011 / Accepted: 1 February 2012 / Published online: 19 February 2012
© Akadémiai Kiadó, Budapest, Hungary 2012

Abstract The oxidation, in a neat oxygen atmosphere, of high-purity and highly crystalline natural graphite and synthetic Kish graphite was investigated. The physico-geometric model function of the kinetic rate equation was experimentally determined by isothermal thermogravimetric analysis at 650 °C. Analytic solutions for basic flake shapes indicate that this function strictly decreases with conversion. However, for both samples the experimental data trend was a rapid initial increase followed by the expected decrease to zero. High resolution field emission scanning electron microscopy, of partially oxidized flakes, provided plausible explanations for this discrepancy. Rapid development of macroscopic surface roughness during the initial stages of oxidation was evident and could be attributed to the presence of catalytic impurities. Large fissures along the planes of the natural graphite and the initiation, growth and coalescence of internal cavities in the Kish graphite were observed. Flake models incorporating the latter two features are difficult to analyse analytically. However, a facile probabilistic approach showed that reasonably good agreement with experimental data was possible.

Keywords Graphite · Oxidation · Thermal analysis · Modelling · Simulation

Introduction

The Pebble Bed Modular Reactor (PBMR) is a High Temperature Gas Cooled Reactor (HTGR) design that incorporates numerous inherent passive safety features. Graphite is an important material of construction for the reactor core and the fuel pebbles. Knowledge of the high temperature oxidative behaviour of the graphite materials utilized in such reactors is important for design and accident modelling purposes [1, 2]. The nuclear fuel is embedded in a graphite matrix to form the pebbles. Both natural and synthetic graphite powders are used as fillers in the matrix. This study represents a small step towards developing an understanding of the factors controlling the oxidation kinetics of typical graphite constituents.

Thermal analysis (Thermogravimetry (TG), Derivative Thermogravimetry (DTG), Differential Thermal Analysis (DTA), Differential Scanning Calorimetry (DSC), etc.) is widely utilized to determine kinetic rate parameters for gas–solid reactions. Such reactions are frequently modelled using a differential equation of the following form [3, 4]:

$$\frac{d\alpha}{dt} = kf(\alpha) P_{O_2}^r \quad (1)$$

where α is the dimensionless degree of conversion or reaction; t is the reaction time; k is the temperature dependant reaction rate constant; $f(\alpha)$ is the physico-geometric reaction model or conversion function; and P_{O_2} is the partial pressure of the reacting gas (in this case oxygen) while r is the gas-phase reaction order. Hurt and Haynes [5] pointed out that the simple order term describing the influence of the reacting gas is unexpected for a complex reaction in which the adsorption/desorption of oxidative species, the energetic distribution of surface complexes and the competition with gaseous inhibitor

H. Badenhorst · W. W. Focke (✉)
SARChI Chair in Carbon Technology and Materials, Institute of Applied Materials, Department of Chemical Engineering, University of Pretoria, Pretoria 0002, South Africa
e-mail: walter.focke@up.ac.za

species all play a role. Nevertheless, for the C–O₂ reaction there is compelling evidence that a simple order parameter satisfactorily represents the influence of the oxygen's partial pressure on the overall reaction rate [5].

The experimental difficulties associated with the execution of precise isothermal TG and DSC experiments with gas–solid reactions are well known [3, 6–8]. The difficulty associated with both isothermal and non-isothermal approaches however, is the correct choice of the form of the conversion function to fit the experimental data. Most kinetic studies of the reaction of graphite with oxygen were limited to determining the kinetic parameters for the initial reaction rates [9, 10] or focussed on the reaction order of oxidant gas pressure [11, 12]. Few studies considered characterizing graphite powders. Instead they focused on the solid synthetic graphite reflector blocks which are used directly in the reactor. Oxidation rate of such blocks is affected by the development of internal porosity and other geometric factors [10]. It was found to be limited by diffusion even at fairly low temperatures (~600 °C) [13]. These effects are not expected to be significant for the small samples of micrometer-sized powders with narrow particle size distributions considered presently.

Walker and co-workers [14, 15] identified the importance of the active surface area (ASA) in the C–O₂ reaction and the difficulty of obtaining unambiguous values experimentally. However, the nature of the intrinsic conversion function relevant to graphite oxidation is an aspect that has received relatively little attention. Thus, the aim of this study was to use isothermal thermal analysis methods to characterize the chemical oxidation kinetics (i.e. in the absence of mass transfer limitations) of two proprietary graphite samples, not only in the initial stages of burn-off, but also across the entire range of conversion. Ultimately the end goal is to establish appropriate conversion function models for graphite oxidation and hence identify the underlying mechanisms that govern the reaction.

Experimental

Two types of high purity graphite were used in this study. Large flakes of highly crystalline synthetic Kish graphite were obtained from Convalent Materials Corporation. In this case, the flakes (~1 mm) were individually selected and oxidized. High purity (>99.9 wt%) natural graphite flakes were supplied by Graphit Kropfmühl AG. This powder was sieved and a narrow particle size fraction (100–150 µm) was collected for further analysis.

The graphite samples were isothermally oxidized in pure oxygen using a TA Instruments SDT Q600 thermogravimetric analyser (TG) under atmospheric pressure. Powdered samples (*ca.* 1 mg) were placed on open 90 µL

platinum pans. The runs were started with the temperature at 25 °C and instrument grade argon flowing at 300 mL/min. The samples were heated to the measurement temperature at a scan rate of 10 °C/min and held there for 15 min. Then the argon flow was shut off and oxygen (instrument grade min 99.5% purity) flow was started at 300 mL/min. The experiment was repeated three times for each graphite sample. The response detected by the mass spectrometer (Pfeiffer QMS 200) connected to the furnace outlet showed that the dynamics of the gas change, from inert to reactive, was quick and characterised by a first-order process with a time constant of $\tau \approx 2.6$ min.

SEM images were obtained using an ultrahigh resolution field emission SEM (HR FEGSEM Zeiss Ultra Plus 55) with an InLens detector at acceleration voltages as low as 1 kV to ensure maximum resolution of surface detail.

Results

Figure 1 shows a SEM picture of an as-received natural graphite flake and Fig. 2a partially oxidized flake. Several linear fissures are evident on the surface of the flake planes in the latter picture. Despite the stated high purity, SEM imaging revealed the presence of some residual catalytic impurities (Fig. 3). The catalytic impurities affected the development of ASA of the as-received sample in a complex manner. A variety of different behaviours were observed ranging from channelling and edge roughening to pitting. They promoted macroscopic surface roughening during oxidation. See Fig. 4. The formation and growth of internal pits was a feature common to both graphite samples. See Fig. 5.

Previous experimental investigations of graphite oxidation revealed that the shape of the conversion function is approximately independent of the isothermal measurement temperature [16]. Thus, Fig. 6 only reports the conversion

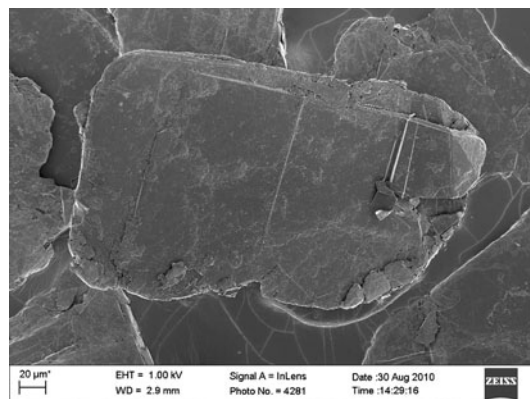


Fig. 1 SEM picture of as-received natural graphite flake showing crystal twinning on the top surface

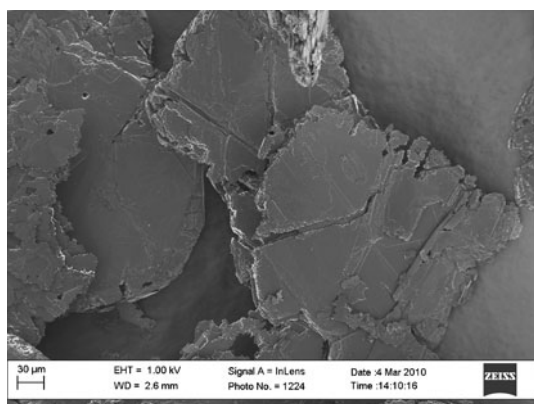


Fig. 2 High resolution SEM picture of a natural graphite flake partially oxidized at 500 °C. Note the presence of fissures on the top surface

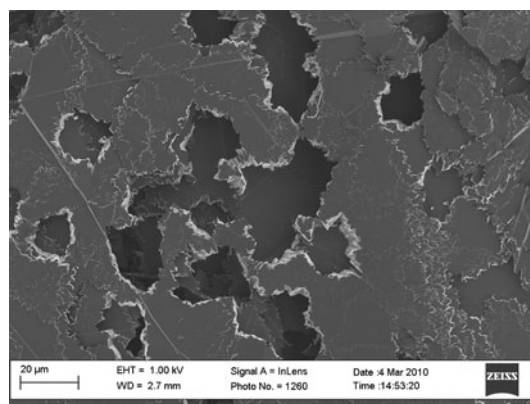


Fig. 5 SEM picture of purified natural graphite flake partially oxidized at 650 °C showing the growth and coalescence of internal pits

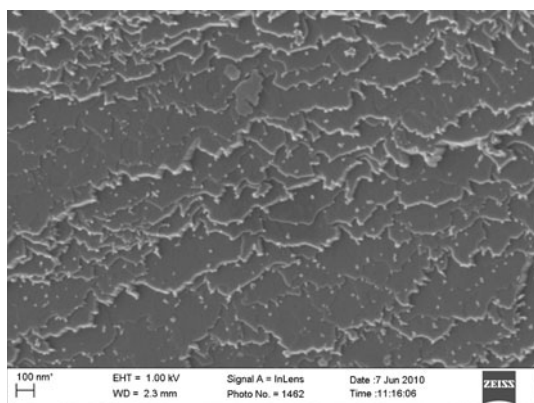


Fig. 3 High resolution SEM picture of as-received natural graphite flake at 2.5% burn off at 650 °C. The small ‘dots’ are the catalyst particles

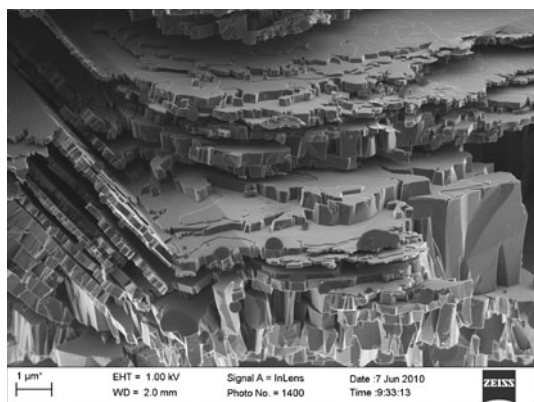


Fig. 4 High resolution SEM picture of as-received natural graphite flake at ca. 50% burn off at 650 °C. The small ‘dots’ are catalyst particles

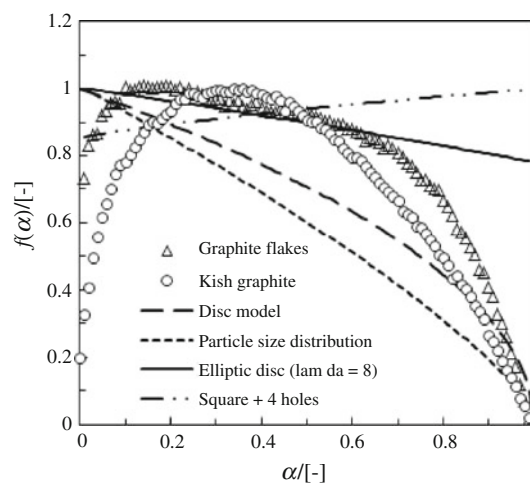


Fig. 6 Scaled reaction rate curves for Kish graphite and natural graphite flakes oxidized at 650 °C in oxygen. The experimental data are compared to analytical expressions for a circular disc; a linear decreasing particle size distribution of disc shaped particles and an elliptical disc with aspect ratio $\lambda = 8$

function for the two graphite samples obtained by isothermal oxidation runs conducted at 650 °C. It also compares the experimental data with predictions based on

analytic solutions derived for simple geometric models. It is clear that the actual burn off behaviour of both graphite samples differed greatly from the predictions. The analytic solutions feature burn off functions that either increase or decrease with the degree of conversion. In contrast, the experimental data revealed well defined maximum rates at intermediate degrees of burn off. Clearly, the reasons for the discrepancy are linked to the features observed in the SEM pictures presented in Figs. 1, 2, 3, 4 and 5. The geometry and the ASA development in the real samples are significantly more complex than predicted by the idealized disc shape. In the case of the natural graphite, the presence of large fissures which cut across the overall flake shape (Fig. 1) was the prominent feature. These were attributed to the impurities present within the original graphite crystals during their natural formation. On the other hand, the

development of a few distinct, large pits within the flake structure was the most notable feature in Kish graphite. The consequence of these and other geometric characteristics of the flakes on the burn off function are presented below. They were explored by a systematic analysis of the effects of particle shape (including aspect ratio), particle size and particle size distribution and internal cavities. The effect of surface roughness development is only briefly considered here as a more detailed analysis of this factor will be presented in a separate communication. First simple analytic expressions are considered and then the utility of a probabilistic numerical simulation of burn off behaviour is presented.

Analytic models

The unique feature of the oxidation of graphite flakes is that the oxidation proceeds at the exposed edges only, i.e. it is fundamentally a two-dimensional process. Consider an oxidation reaction that is kinetically rather than mass transfer controlled. This implies that at any point, under isothermal conditions, the edge of a graphite flake recedes at a constant velocity, v , when measured in the direction of the normal to the surface at that point.

Uniform oxidation of a circular disc

Consider an idealized circular graphite flake with initial diameter D_o and thickness h . In this case, geometric similarity is maintained during burn off as the reaction proceeds smoothly and homogeneously at the disc edge only. For this disc-shaped flake the reactive surface area (A) and mass (m) are given by

$$A = \pi Dh \quad (2)$$

$$m = \frac{\pi}{4} \rho_c D^2 h \quad (3)$$

where ρ_c is the crystal density of perfect graphite. Geometric considerations allow the reactive surface area to be expressed in terms of conversion. The subscript 'o' is used to denote the values that variables held at the start of the reaction. Since the reaction only proceeds from the edges, the thickness remains constant throughout. Hence, the degree of conversion may be written as

$$\alpha \equiv 1 - m/m_o = 1 - D^2/D_o^2 \quad (4)$$

During the reaction the diameter decreases at a constant rate according to

$$\frac{dD}{dt} = -2v \quad (5)$$

Equations 4 and 5 can be combined to read

$$\frac{d\alpha}{dt} = \frac{4v}{D_o} \sqrt{1-\alpha} \quad (6)$$

Solving the differential equation yields

$$\alpha = 1 - (1 - 2vt/D_o)^2 \quad (7)$$

The reaction reaches completion after time equal to $\tau = D_o/(2v)$ has elapsed. Thus, the reaction time scales linearly with flake size. Since the reaction only occurs at the flake edge, it is actually more appropriate to use the flake perimeter, rather than the diameter of the disc, as the scaling length:

$$\frac{d\alpha}{dt} = \frac{4\pi v}{C_o} \sqrt{1-\alpha} = k\sqrt{1-\alpha} \quad (8)$$

The conversion function corresponds to a dimensionless reaction rate. For an isothermal oxidation of a given sample, it is obtained by dividing throughout with the constant k on the right hand side of Eq. 8. The normalized conversion function for the idealized disc shape is plotted in Fig. 6. According to Eqs. 6 and 8 the burn off rate is at a maximum at the start of the reaction and then decreases with increasing conversion.

The effect of flake shape

The analytical approach illustrated above can be extended to other basic geometries. The results of such analyses are presented in Table 1 and in Table 2. The effect of shape can be illustrated by considering a regular convex polygon with n equal-length sides. Analysis along the lines presented above yields

$$\frac{d\alpha}{dt} = \frac{4v \sec(\pi/n)}{d_o} \sqrt{1-\alpha} = \frac{4vn \tan(\pi/n)}{C_o} \sqrt{1-\alpha} \quad (9)$$

The values of the quantities $\sec(\pi/n)$ and $n \tan(\pi/n)$ are listed in Table 1 for selected geometric shapes. Equation 10 shows that the burn off functions for regular convex polygons differ from that for the circular disc only with respect to constant multipliers.

The effect of flake aspect ratio

Entries I and II in Table 2 show the effect of flake aspect ratio on the form of the rate equation for rectangular and elliptical flakes. The corresponding expressions demonstrate that the burn off rate becomes less sensitive to the degree of conversion as the aspect ratio increases. This also applies to square flakes with two short sharp notches (entry III in Table 2), but the opposite is true for the Swiss cross-shaped flake, entry IV in Table 2. If the circular and rectangular discs are given 'concentric' internal holes (entries V and VI in Table 2), the rate expression becomes

Table 1 The values of $\sec(\pi/n)$ and $n \tan(\pi/n)$ for regular convex polygons

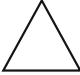
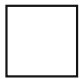



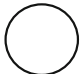
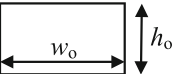
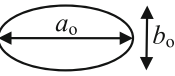
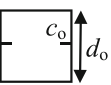
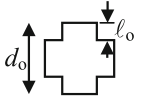
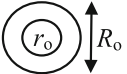
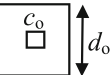
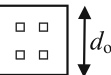
n	Shape	Name	$\sec(\pi/n)$	$n \tan(\pi/n)$
3		Isosceles triangle	2	5.196152
4		Square	1.414214	4
5		Pentagon	1.236068	3.632713
6		Hexagon	1.154701	3.464102
8		Octagon	1.082392	3.313708
∞		Circular disc	1	π

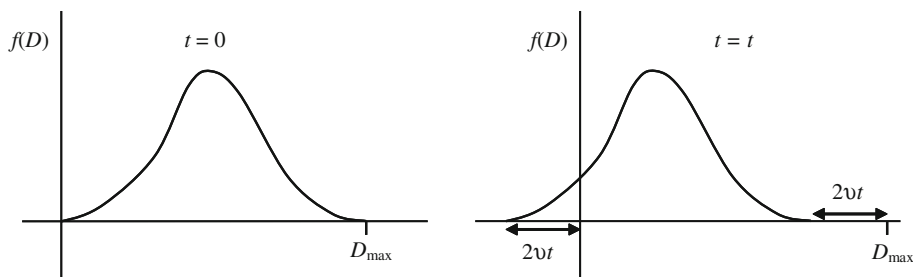
Table 2 Analytic rate expressions for selected geometries

#	Shape	Rate equation	Comment
I		$\frac{dz}{dt} = \frac{8v}{C_o} \sqrt{\lambda} \left(1 + \frac{1}{\lambda}\right) \sqrt{\frac{(1+\lambda)^2}{4\lambda} - \alpha}$	$\lambda = w_o/h_o \geq 1$
II		$\frac{dz}{dt} \approx \frac{2\sqrt{2}\pi v}{C_o} \sqrt{\lambda + 1/\lambda} \sqrt{\frac{(1+\lambda)^2}{4\lambda} - \alpha}$	$\lambda = a_o/b_o \geq 1$
III		$\frac{dz}{dt} \approx \frac{16v}{C_o - 2c_o} \sqrt{(1 + \delta^2) - \alpha}$	$\delta = c_o/d_o \leq 1/4$
IV		$\frac{dz}{dt} \approx \frac{16v}{C_o} \sqrt{(1 - 4\delta^2) - \alpha}$	$\delta = l_o/d_o \leq 1/4$
V		$\frac{dz}{dt} = \frac{4\pi v}{(C_o - \pi c_o)(1 - \delta)}$	$\delta = r_o/R_o$ $C_o = \pi(R_o + r_o)$
VI		$\frac{dz}{dt} \approx \frac{16v}{(C_o - 4c_o)(1 - \delta)}$	$\delta = c_o/d_o$ $C_o = 4(d_o + c_o)$
VII		$\frac{dz}{dt} \approx \frac{16v}{C_o} [5 + \sqrt{1 + 3\alpha}]$	Four internal square holes initially infinitesimally small and positioned equidistant from nearest edges and neighbours

independent of conversion: The decrease in reactive surface area at the edges is perfectly compensated by a corresponding increase in the reactive surface area of the

internal hole. However, for the specific flake design featuring multiple internal cavities (entry VII in Table 2) the surface area available for reaction increases with

Fig. 7 The effect of burn off on the particle size distribution of disc-shaped powder. The oxidation reaction proceeds at a rate such that the disc diameter decreases by a rate equivalent to $2v$



conversion. So, multiple cavities growing inside a flake provides a basis for the observation that the burn off rate increases during the initial stage of the reaction. This rate can reach a maximum and then decline when these internal openings coalesce into fewer cavities and/or merge with the flake edges. This is demonstrated by a simulation presented in the next section.

The effect of particle size distribution

The effect of particle size distribution on the burn off behaviour was analysed using circular disc-shaped flakes. This choice for the flake shape was a matter of convenience as it greatly simplifies the derivation of the burn off function. Consider an arbitrary initial particle size distribution as shown in Fig. 7. After a time $t = t$, every disc diameter has decreased by an amount $-2vt$. The new distribution can be found by simply shifting the original one to the left by this same amount as indicated in Fig. 7. Since the mass of particles remaining is proportional to the weighted square mean of diameters, the degree of conversion at time $t = t$ is given by

$$1 - \alpha = \frac{D_{\max}^2}{\langle D^2 \rangle} \int_0^{1-z} x^2 f(x+z) dx \tag{10}$$

where

$$z = 2vt/D_{\max} \text{ and } \langle D^2 \rangle = D_{\max}^2 \int_0^1 x^2 f(x) dx \tag{11}$$

The binomial distribution provides a flexible continuous probability distribution with the advantage that particle's size range is limited to a fixed range $0 < d < d_{\max}$. It includes other, much simpler distributions as special cases as shown in Fig. 8. The pertinent expression for the parameter $x = d/d_{\max}$ is

$$f(x) = \frac{\Gamma(p+q)}{\Gamma(p)\Gamma(q)} (x)^{p-1} (1-x)^{q-1} \quad 0 \leq x \leq 1 \tag{12}$$

with $p, q > 0$; mean particle size $\langle D \rangle = \frac{p}{p+q} D_{\max}$ and standard deviation $\sigma = \frac{pqD_{\max}}{(p+q)^2(p+q+1)}$.

Analytic expressions for the rate equation are possible for limiting forms of the distribution. The uniform distribution (distribution *b* in Fig. 8) is obtained for $p = q = 1$. Application of Eqs. 10 to 12 yields

$$\frac{d\alpha}{dt} = \frac{6v}{D_{\max}} (1 - \alpha)^{2/3} \tag{13}$$

The linear decreasing distribution, distribution *a* in Fig. 8, results in

$$\frac{d\alpha}{dt} = \frac{8v}{D_{\max}} (1 - \alpha)^{3/4} \tag{14}$$

The analytical results obtained for the simple geometries analysed here, and reported in Table 2, can be summarized with the general expression:

$$\frac{d\alpha}{dt} = k(a_1 \mp \alpha)^n + a_2 \tag{15}$$

With the exception of multiple cavities, the negative sign applies. The constants k, a_1 and a_2 are functions of flake geometry. For simple rotationally symmetric flake shapes corresponding to convex n -polygons, $a_1 = 1, a_2 = -1$ and $n = 1/2$. The constant a_1 is affected by flake aspect ratio. It also differs from unity for flakes with an

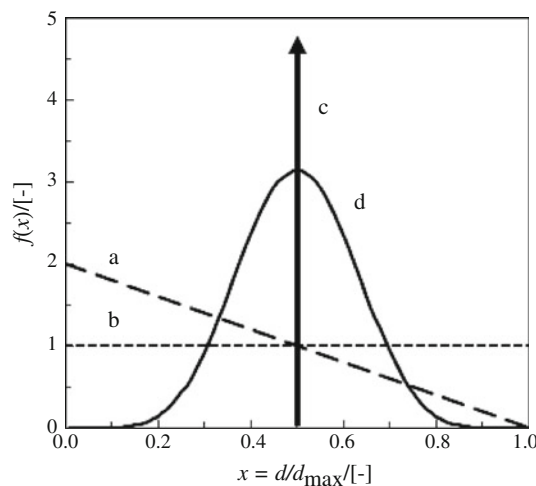


Fig. 8 Representative particle size distributions based on the Binomial distribution, Eq. 12: (a) Linear decreasing ($p = 1; q = 2$); (b) Uniform ($p, q = 1$); (c) Monodisperse particle size ($p, q \rightarrow \infty$); and (d) Binomial with $p, q = 8$

irregular shape or flakes with internal flaws. Often the exponent $n = 1/2$ but it equals zero when a concentric hole is present in a disc. The exponent n assumes larger values when a uniform or linearly decreasing particle size distribution applies. The exponent n in Eq. 11 is affected by the shape of the particle size distribution. A linear burn off is observed as n approaches unity. The point is that the particle size distribution does affect the conversion function for a powder. In general, it is expected that the burn off behaviour will show a much more complicated functional dependence on α when the particles either have a more complex shape or size distribution.

The fate of surface irregularities

If burn off indeed occurred homogeneously, then it is expected that the reactive boundary should become smoother as the reaction proceeds, e.g. protrusions would disappear over time. For example, when the apex of the rectangular edge in Fig. 9 has descended a distance $h + s = \sqrt{2} vt$, the linear edge will have travelled a distance $s = vt$ in the same time interval. This means that the protrusion disappears just at the point when the linear edge has progressed a distance $s = h/(\sqrt{2} - 1)$. However, this does not accord with the experimental observations because of the catalytic effect of impurities.

Catalyst channelling

Catalytic oxidation of graphite has received considerable attention [17–19]. Ranish and Walker [17] considered the effect of catalyst particles on the development of ASA. The present focus is to study the effect of pitting on the conversion function. When a catalyst particle is present, the key outcome is that it cuts a swath through the flake thereby generating more ASA for the non-catalysed reaction to proceed. Figure 10 shows an idealized situation for a single catalyst particle channelling directly into a graphite flake. In a time interval Δt the surface moves a distance $s = v\Delta t$ to the right. During the same time, the catalyst particle moves from its initial position (point A) at

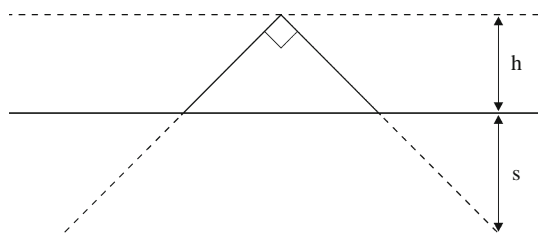


Fig. 9 Vanishing of an isolated rectangular protrusion located at a straight edge. The protrusion disappears when the linear edge has moved a distance $s = h/(\sqrt{2} - 1)$

the surface to an internal location (point B). It is assumed that the velocity of the catalyst particle is a multiple λ of that of the rate of surface recession, i.e. $U = \lambda v$. As the catalyst particle cuts into the flake, it opens up fresh surface making it available for oxidation. When the relative rate of particle penetration is very high, the channel shape is approximately triangular. The apex angle θ is linked to the relative velocities of surface recession to that of the catalyst by the expression: $\tan \theta/2 = 1/\lambda$. After a time t , the catalyst region of influence corresponds to a width $2s = 4vt$ at the original position of the interface. In the absence of the catalyst particle, the size of the local area that would be oxidized anyway therefore equals $2s^2$. The presence of the catalyst causes an additional loss corresponding to the surface area of the triangular cavity. The local rate enhancement can be taken to be proportional to the surface area graphite removed relative to the one that would have been removed anyway. This local rate enhancement by a single catalyst particle is approximately given by

$$K_1 = v_1/v_0 = (\lambda + 1/\lambda)/2 \tag{16}$$

where v_0 and v_1 are the apparent local surface recession rates in the absence of catalyst, and in the presence of a catalyst particle, respectively. Note that Eq. 16 indicates that a catalytic rate enhancement requires a catalyst penetration rate (U) that exceeds that of the intrinsic rate (v_0) at which the surface recedes, i.e. $\lambda > 1$. Note also that for $\lambda \gg 1$, $K_1 \approx \lambda/2$.

This rate enhancement K_1 is the maximum initially possible for a regularly spaced array of catalyst particles, placed along the initial surface at a distance $2s$ apart, that channel straight into the flake interior. In reality, the rate enhancement will be less. Catalyst particles would generally occupy random positions and be present everywhere as inclusions; those at the surface will penetrate at different angles and may even change direction. Their spheres of influence will eventually overlap and catalyst particles could also meet, coalesce and even become deactivated. However, it is clear that the presence of catalyst particles

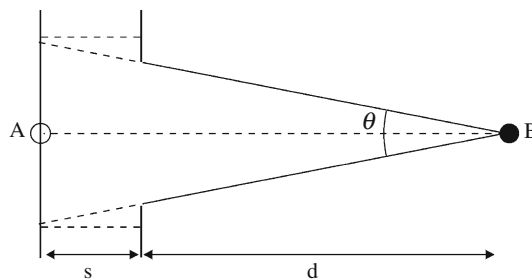


Fig. 10 Isolated catalyst particle burrowing into the flake interior. This is approximated as a triangular cavity but in actual fact the cavity walls have curvature

enhances the rate of oxidation. There is initial rate acceleration owing to the creation of macroscopic surface roughness and a sustained rate enhancement owing to the continued action of the catalyst particles. Consider the effect of increasing the concentration of catalyst particles. As more and more are added, their spheres of action will increasingly overlap with those of other particles already present. Beyond a certain critical concentration one expects that no further rate enhancement will occur and that the sustained rate enhancement will reach a saturation level that is independent of catalyst concentration. Since each catalyst particle performs a 'random walk' on the Cartesian plane, it is reasonable to assume that the rate enhancement caused by a swarm of catalyst particles might be given by an expression of the form

$$K_{\infty} = v_{\infty}/v = K_1^m \quad (17)$$

where m is an exponent less than unity but probably greater than a half.

Note that this analysis assumes that the catalytic effect of enhancing the reaction rate is a local one confined to the vicinity of the flake boundaries. This means that the effect of the macroscopic flake geometry is retained and that the same equations still apply except that the recession velocity must be adjusted, i.e. the intrinsic recession velocity (v) applicable to the situation where no catalyst is present must be replaced by the apparent catalysed value (v_{∞}):

$$v_{\infty} = vK_{\infty} = v(\lambda/2)^m = 0.5^m v^{1-m} U^m \quad (18)$$

Both the natural oxidation and the catalyst penetration velocities result from activated processes, each with their own activation energies. Equation 18 predicts that the effective activation energy (E_e) for a catalytic oxidation contains weighted contributions from the activation energy (E_o) for the catalyst-free intrinsic oxidation velocity and that for a catalyst particle (E_c):

$$E_e = (1 - m)E_o + mE_c \quad (19)$$

A more detailed analysis of the effect of catalytic particles on the rate of graphite oxidation will be presented in a separate communication.

Numerical simulation

The derivation of analytical expressions for very complex morphologies becomes tedious and impractical. Even if an analytic solution is possible, its form may become so complicated as to obscure the expected trend. Graphical representations are much easier to understand and interpret and they can be generated even in the absence of analytical equations. Arbitrary surface geometries are easily simulated using a probability based method. The oxidation of a flake

with such a given starting geometry is readily simulated using a random number generator combined with a recipe for calculating the probability that a given element will react during the simulation. Nearly any geometry imaginable, comprising either a single sheet or three dimensional stacks of sheets, each with its own shape, can be constructed. The chosen geometrical shape is subdivided into a grid pattern similar to conventional finite element analysis. In this investigation, the sheets were discretized using a Cartesian grid with mesh size δ , i.e. using square elements for a 2-D simulation. Cubic elements can be used to simulate 3-D structures.

The simulations considered cyclic removal of edge elements based on their exposed surface, i.e. reactive edge length. An arbitrary probability of removal (P_1) is assigned to a single exposed edge per cycle. This probability is linked to the edge recession velocity by the expression: $v = P_1 \delta f$ where v is the burn off velocity in m.s^{-1} ; f is the cycle frequency measured in Hz, and δ is the grid edge length measured in m. Since it is assumed that the reaction only occurs at the edges, each element has at most four edges that can be attacked. The probability that an element with n exposed surface will react in a cycle is given by $P_n = 1 - (1 - P_1)^n$. Note that $P_0 = 0$ because only elements with exposed edges (or edge faces for 3-D simulations) can react. In this way, a nonzero probability of reaction is assigned to all the elements with exposed edge faces comprising the chosen geometric structure. A random number generator was used to determine whether a given element has reacted during any given cycle. Every element for which the probability of reaction was greater than the number between 0 and 1 generated in that cycle was judged to have reacted and was removed in that cycle. This process was repeated until all the elements were removed. This generated a data set linking the degree of conversion with time. The former is defined as $\alpha = 1 - N(W)/N_o$ where N_o represents the initial number of elements present and $N(W)$ is the number of elements remaining after W cycles. The elapsed time is given by $t = W/f$. The simulation was repeated several times for each geometry investigated, and the results averaged. The predicted conversion rate was then determined from the averaged information using numerical differentiation and a normalized version of $f(\alpha)$ plotted versus α . Note that, provided the mesh size is sufficiently fine, the outcome of this averaged result is independent of the magnitude of the probability P_1 that is selected in the simulation. However, choosing a coarse mesh for the discretization yields an artificially serrated flake boundary. This artificial surface roughness increases the reactive surface area. The consequence is that the simulation predicts faster burn off rates than expected. Simulations using a circular disc were used to optimize grid size and to correct for these effects.

As mentioned earlier, the purified natural graphite distinctly showed the presence of large fissures within the flake macro structure. A probability simulation using the simplified geometric approximation of this case is shown in Fig. 11. As seen from this Figure, the simulation with model geometry provided a useful approximation to the real data.

During oxidation the Kish graphite flake develops holes. A simulation using a simplified approximation comprising a rectangular plate with five randomly placed holes is shown in Fig. 12 provides a good match with the experimental data.

The probability based modelling approach is so flexible that it can be extended in a straight forward manner to include the action of catalytic impurities. This potentially provides a method that could be used fruitfully to study and quantify the effect of impurities on oxidation behaviour. For example, catalyst particles may be approximated as individual

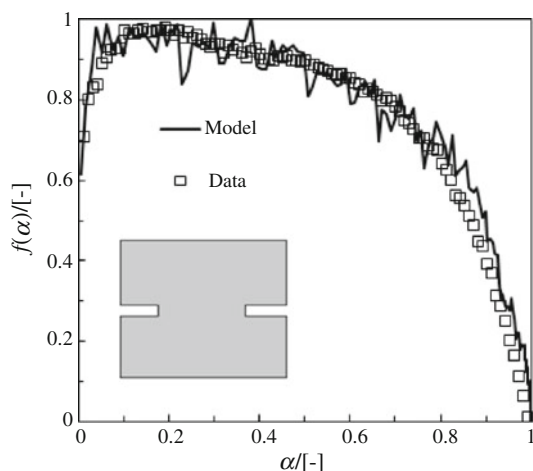


Fig. 11 Simulation based on a simplified model of two fissures in a natural graphite flake (1000 × 1000 grid)

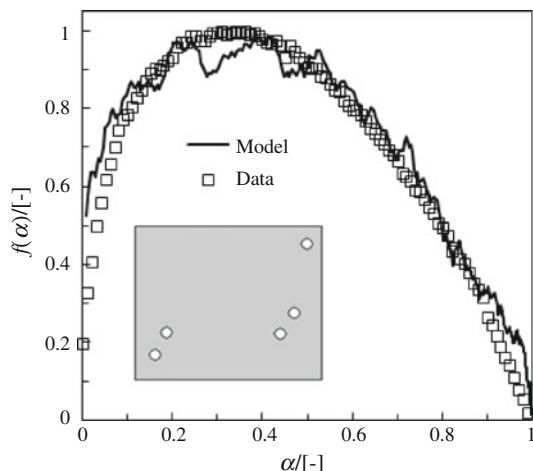


Fig. 12 Kish graphite data and results of a model based on a rectangular flake with five, randomly placed holes (1000 × 1000)

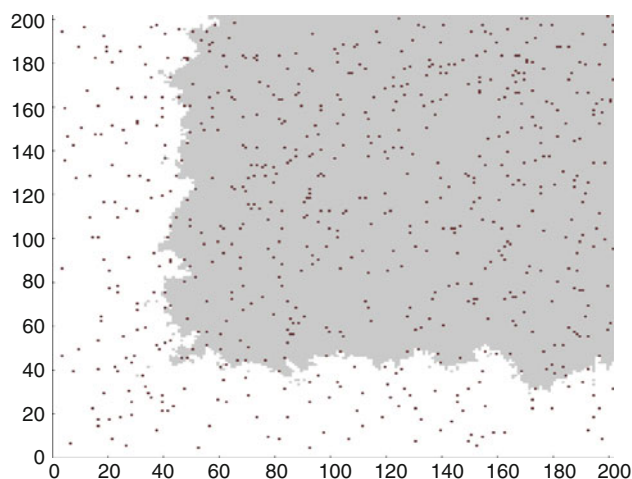


Fig. 13 Surface patterns obtained with a probabilistic simulation of catalytic oxidation. The catalyst particles, indicated by the red squares, randomly attack the graphite creating the erratic edge patterns' characteristic of the catalysed oxidation of graphite. (1000 × 1000 grid). (Color figure online)

subelements within the finite element grid. These subelements are free to move into any adjacent grid location where graphite is present; removing it from the simulation as though it had been oxidized. Different probabilities can be used to determine whether a given graphite subelement or catalyst subelement reacts within a given time step. This allows direct tuning of the relative reactivity of the catalysed and uncatalysed reactions. An additional random number generator can be included, which used allow a catalyst particle to change direction. This facilitates random walks for the catalyst particle over the graphite surface. A sample simulation is presented in Fig. 13. The catalyst particles, indicated by the red squares, randomly attack the graphite creating the erratic edge patterns' characteristic of the catalysed oxidation of graphite. The evolving surface pattern closely resembles actual SEM images of catalytically oxidized flakes. It is hoped that this simulation can be extended in future to provide insights into the effect on the activation energy of the catalysed oxidation.

The numerical simulations presented above did not consider the catalytic effect as this is the subject of future work. However, the granularity of the finite-sized elements used, in effect, also leads to the development of an irregular edge boundaries during the early stages of oxidation. The end effect is behaviour akin to the surface roughness introduced by the catalyst particles.

Conclusions

The oxidation rate of two high-purity, highly crystalline, graphite samples was determined as a function of

conversion using isothermal thermogravimetric analysis at 650 °C. Changes in the morphologies of the flakes, due to the oxidation reaction in pure oxygen, were studied by high resolution field emission scanning electron microscopy (FEGSEM). Both samples developed macroscopic surface roughness during the initial stage of oxidation. This was attributed to the presence of catalytic impurities. However, the success of a probabilistic modelling approach suggested that the physico-geometric model function of the kinetic rate equations was dominated primarily by the effect of two other morphological features that were observed by FEGSEM. In the case of the synthetic Kish graphite sample it was the formation, growth and coalescence of internal cavities. In contrast, a simple model of a flake with two large fissures reproduced the oxidation rate trends shown by the natural graphite. These conclusions are based on simulations that utilized simplistic but plausible approximations of the actual flake starting morphologies.

The probabilistic modelling approach allows any imaginable geometry to be simulated. This includes the effect of catalytic impurities as preliminary results indicate that the model is capable of replicating the erratic edge roughness characteristic of the catalysed oxidation of graphite. Thus the approach is, in principle, capable of modelling the relevant mechanisms which control the reaction rate during the oxidation of graphite. It can be concluded that the probability based model developed and presented here can be used fruitfully to explore the burn off behaviour of arbitrary shapes. Simulations based on simple geometric models that qualitatively reproduced characteristic features observed by electron microscopy yielded semi-quantitative agreement with experimentally observed burn off behaviour. These simulations support the hypothesis that, for highly pure and highly crystalline graphite samples, the conversion function is solely governed by the development of complex active surface area geometries including fissures and internal cavities. Furthermore, this approach allows quick and easy modelling of the progression of these geometries that would be difficult to achieve by analytical modelling.

Acknowledgements This work is based upon research supported by the Skye Foundation, PBMR and the South African Research Chairs Initiative of the Department of Science and Technology and the National Research Foundation. Any opinion, findings and conclusions or recommendations expressed in this material are those of the authors and therefore the PBMR, NRF and DST do not accept any liability with regard thereto.

References

1. De Torre LEC, Llanos JL, Bottani EJ. Graphite oxidation in air at different temperatures. *Carbon*. 1991;29:1051–61.
2. Fuller EL, Okoh JM. Kinetics and mechanisms of reaction of air with nuclear grade graphites: IG-110. *J Nucl Mater*. 1997;240:241–50.
3. Šesták J, Berggren G. Study of the kinetics of the mechanism of solid-state reactions at increasing temperatures. *Thermochim Acta*. 1971;3:1–12.
4. Koga N. Physico-geometric kinetics of solid-state reactions by thermal analyses. *J Therm Anal*. 1997;49:45–56.
5. Hurt RH, Haynes BS. On the origin of power-law kinetics in carbon oxidation. *Proc Combust Inst*. 2005;30:2161–8.
6. Feng B, Bhatia SK. On the validity of thermogravimetric determination of carbon gasification kinetics. *Chem Eng Sci*. 2002;57:2907–20.
7. Koga N, Tanaka H. A physico-geometric approach to the kinetics of solid-state reactions as exemplified by the thermal dehydration and decomposition of inorganic solids. *Thermochim Acta*. 2002;388:41–61.
8. Gimzewski E. The relationship between oxidation induction temperatures and times for petroleum products. *Thermochim Acta*. 1992;198:133–40.
9. Zaghbi K, Song X, Kinoshita K. Thermal analysis of the oxidation of natural graphite: isothermal kinetic studies. *Thermochim Acta*. 2001;371:57–64.
10. Kim ES, Lee KW, No HC. Analysis of geometrical effects on graphite oxidation through measurement of internal surface area. *J Nucl Mater*. 2006;348:174–80.
11. Gulbransen EA, Andrew KF, Brassart FA. The oxidation of graphite at temperatures of 600° to 1500 °C and at pressures of 2 to 76 Torr of Oxygen. *J Electrochem Soc*. 1963;110:476–83.
12. Gulbransen EA, Andrew KF. Reactions of artificial graphite: kinetics of oxidation of artificial graphite at temperatures of 425° to 575 °C and pressures of 0.15 to 9.8 cm of mercury of oxygen. *Ind Eng Chem*. 1952;44:1034–8.
13. Xiaowei L, Jean-Charles R, Suyuan Y. Effect of temperature on graphite oxidation behaviour. *Nucl Eng Des*. 2004;227:273–80.
14. Laine NR, Vastola FJ, Walker PL Jr. Importance of active surface area in the carbon-oxygen reaction. *J Phys Chem*. 1963;67:2030–4.
15. Walker PL Jr, Taylor RL, Ranish JM. An update on the carbon-oxygen reaction. *Carbon*. 1991;29:411–21.
16. Badenhorst H, Rand B, Focke WW. Modelling of natural graphite oxidation using thermal analysis techniques. *J Therm Anal Calorim*. 2010;99:211–28.
17. Ranish JM, Walker PL Jr. Models for roughening of graphite during its catalyzed gasification. *Carbon*. 1990;28:887–96.
18. Hennig GR. Catalytic oxidation of graphite. *J Inorg Nucl Chem*. 1962;24:1129–37.
19. McKee DW, Chatterji D. The catalytic behaviour of alkali metal carbonates and oxides in graphite oxidation reactions. *Carbon*. 1975;13:381–90.